Clim. Past Discuss., 8, 5545–5581, 2012
www.clim-past-discuss.net/8/5545/2012/
doi:10.5194/cpd-8-5545-2012

Climate of the Past Discussions

Using data assimilation to investigate the causes of Southern Hemisphere high latitude cooling from 10 to 8 ka BP

P. Mathiot[1,*], H. Goosse[1], X. Crosta[2], B. Stenni[3], M. Braida[3], H. Renssen[4], C. VanMeerbeek[4], V. Masson-Delmotte[5], A. Mairesse[1], and S. Dubinkina[1]

[1]Université catholique de Louvain, Earth and Life Institute, Georges Lemaître Centre for Earth and Climate Research, Place Louis Pasteur, 3, 1348 Louvain-la-Neuve, Belgium
[2]UMR-CNRS EPOC, Université Bordeaux I, Talence, France
[3]University of Trieste, Dipartimento di Matematica e Geoscienze, Trieste, Italy
[4]Cluster Earth & Climate, Department of Earth Sciences, Vrije Universiteit Amsterdam, Amsterdam, The Netherlands
[5]Laboratoire des Sciences du Climat et de l'Environnement (CEA-CNRS-UVSQ/IPSL), Gif-sur-Yvette, France
[*]now at: British Antarctic Survey, Natural Environment Research Council, Cambridge, UK

Received: 26 October 2012 – Accepted: 3 November 2012 – Published: 15 November 2012

Correspondence to: P. Mathiot (pierre.mathiot@bas.ac.uk)

Published by Copernicus Publications on behalf of the European Geosciences Union.

Abstract

Paleoclimate records show an atmospheric and oceanic cooling in the high latitudes of the Southern Hemisphere from 10 to 8 ka BP. In order to study the causes of this cooling, simulations covering the early Holocene period have been performed with the climate model of intermediate complexity LOVECLIM constrained to follow the signal recorded in climate proxies using a data assimilation method based on a particle filtering. The selected proxies represent oceanic and atmospheric surface temperature in the Southern Hemisphere derived from terrestrial, marine and glaciological records. Using our modeling framework, two mechanisms potentially explaining the 10–8 ka BP cooling pattern are investigated. The first hypothesis is a change in atmospheric circulation. The state obtained by data assimilation displays a modification of the meridional atmospheric circulation around Antarctica, producing a 0.6 °C drop in atmospheric temperatures over Antarctica from 10 to 8 ka BP without congruent cooling of the atmospheric and sea-surface temperature in the Southern Ocean. The second hypothesis is a cooling of the sea surface temperature in the Southern Ocean, simulated here as the response to a higher West Antarctic Ice Sheet melting rate. Using data assimilation, we constrain the fresh water flux to increase by 100 mSv from 10 to 8 ka BP. This perturbation leads to an oceanic cooling of 0.5 °C and a strengthening of Southern Hemisphere westerlies (+6 %). However, the observed cooling in Antarctic and the Southern Ocean proxy records can only be reconciled with the combination of a modified atmospheric circulation and an enhanced freshwater flux.

1 Introduction

Over East Antarctica, water stable isotope records from deep ice cores show a temperature optimum around 12–10 ka BP (thousand of years before present, the notation ka is used hereafter) (Masson-Delmotte et al., 2000, 2011; Stenni et al., 2011), followed by a large cooling of about 1 °C from 10 to 8 ka (Fig. 1), which is the strongest millennial Antarctic temperature fluctuation of the last 10 kyr. The mechanisms responsible for this variation have not yet been explored and could be related to changes in atmospheric and/or oceanic circulation, in relationship with changes in orbital forcing and deglacial meltwater fluxes.

In Antarctic coastal regions, only a few quantitative and qualitative sea-surface temperature (SST) and sea ice reconstructions are available. They are based on TEX86 in the West Antarctic Peninsula (Schevenell et al., 2011) and Adélie Land (Kim et al., 2012), on marine diatoms in Adélie Land (Crosta et al., 2008; Denis et al., 2009) and in Prydz Bay (Denis et al., 2010; Barbara et al., 2010) and on lake diatoms in Wilkes Land (Verkulish et al., 2002). These reconstructions from Wilkes Land, Adélie Land and the Antarctic Peninsula similarly suggest a cooling between 10 and 8 ka. The cooling along the Wilkes Land and Adélie Land has been related to glacier advance and sea ice expansion which provided a positive feedback on East Antarctic atmospheric temperature. Along the Antarctic Peninsula, the cooling around 8 ka was suggested to reflect a decrease of Southern Westerlies Wind (SWW), which led to a decrease of Circumpolar Deep Water (CDW) intrusion onto the continental shelf and subsequently a surface cooling (Shevenell et al., 2011).

Conversely, diatom-based reconstructions of sea ice and oceanic temperatures from Prydz Bay suggest that surface waters off Princess Elizabeth Land were warmer at 8 ka compared to 10 ka (Barbara et al., 2010; Denis et al., 2010). This regional warming was suggested to be related to an increase of the CDW intrusion into the shelf between 10 and 8 ka due to a more southern position of the Antarctic Circumpolar Current (ACC).

In the Southern Ocean, in the area between the Antarctic Slope Front (ASF) and the Sub Tropical Front (STF), geological records generally show a large cooling from 10 to 8 ka, similar to the one estimated at the surface of Antarctica (Anderson et al., 2009; Bianchi and Gersonde, 2004; Hodell et al., 2001; Crosta et al., 2005; Panhke and Sachs, 2006; Sicre et al., 2005; Nielsen et al., 2004). The rapid transition is thought to be caused by a northward migration of oceanic fronts (south ACC front, polar front,

sub Antarctic front or STF). Besides, the more gradual cooling observed during the Early Holocene was mainly explained by the precessional insolation. Associated with this cooling event, diatom records in the marine cores located south of the polar front suggest a northward migration of the sea-ice front during the 10–8 ka period (Nielsen et al., 2004; Bianchi et al., 2004; Hodell et al., 2001).

By contrast, one pollen record in the Campbell Island area (McGlone et al., 2010) shows a clear warming from 10 to 8 ka. These authors explained this feature by an equatorward migration and a strengthening of the SWW over Campbell Island and, consequently, an increase in poleward meridional heat transport. This is however inconsistent with nearby SST reconstructions (Crosta et al., 2004; Pahnke and Sachs, 2006), which showed a clear oceanic cooling during the 10–8 ka BP period (Fig. 1).

Our overview of existing early Holocene SH high latitude temperature records shows a large atmospheric and oceanic cooling from 10 to 8 ka. However, the causes of this cooling are not well known. Studies using transient climate simulations have proposed several hypotheses to explained Holocene variability and potentially providing insight on the causes of the cooling between 10 and 8 ka.

Using an intermediate complexity ocean-sea ice-atmosphere model, Renssen et al. (2005) showed that during the Holocene, a delayed response of the Southern Ocean–Antarctic climate to local orbitally-driven insolation changes, with a large influence of the memory of the system. In their simulation, changes in meridional heat fluxes had a negligible impact, as a result of small change in SWW.

Changes in large scale ocean circulation, related to meltwater fluxes in the northern or southern latitudes, can also affect the both atmospheric and sea surface temperatures in the high southern latitudes. While the last glacial period is marked by small maxima in Antarctic temperature associated with a bipolar seesaw with Northern Hemisphere temperature (causing an opposite temperature response at both poles, e.g. Crowley et al., 1992; Stocker, 1998; Capron et al., 2010), similar mechanisms were suggested to account for early interglacial Antarctic warmth (Stenni et al., 2011; Masson-Delmotte et al., 2010; Holden et al., 2010). Such large scale bipolar seesaw inducing austral warmth may be driven by the impact of the final Laurentide meltwater flux on the Atlantic Meridional Overturning Circulation. Additionally, changes in the North Atlantic could also influence high Southern Latitudes through advective oceanic connections (causing then temperature changes of the same sign, Renssen et al., 2010).

Alternatively, the high southern latitude climate can also be strongly affected by the melting rate of the Antarctic ice sheet, as shown for instance in idealized modeling studies (Swingedouw et al., 2009). This local freshwater forcing induces a surface atmospheric and oceanic cooling in the Southern Hemisphere, with the largest signal in the Southern Ocean, where an increase of sea ice cover is simulated, as well as a strengthening of westerlies and easterlies. So far, this mechanism has not been investigated as an explanation for the early Holocene changes around Antarctica.

Using data assimilation in an intermediate complexity climate model, we aim to test the ability of two different hypotheses to explain this cooling: either a change in the atmospheric circulation, or an oceanic cooling caused by a change in the local fresh water flux (fwf).

Today, there is no consensus on the melting of the West Antarctic Ice Sheet (WAIS) during the early Holocene (Bentley et al., 2010; Stone et al., 2003; Domack et al., 2005; Bianchi et al., 2004; Crespin et al., 2012; Pollard et DeConto, 2009; Peltier, 2004; Mackintosh et al., 2011) to justify this choice or to discard it a priori. Thus, the WAIS melting represents here a working hypothesis that allows us modifying in a relatively simple and straightforward way the temperature and the circulation in the Southern Ocean. We do not take into account the East Antarctic Ice Sheet (EAIS) melting because the EAIS is more stable than the WAIS (Bentley, 2010; Sidall et al., 2012) and also because it is admit that the EAIS melting is largely weaker than the WAIS (Pollard et DeConto, 2009; Mackintosh et al., 2011).

To test these two hypotheses, different snapshot simulations are performed with the Earth-System Models of Intermediate Complexity LOVECLIM (Goosse et al., 2010) for 10 and 8 ka. The baseline simulations take into account the different boundary

conditions. New simulations include a data assimilation method which allows combining directly model results and proxy records in order to have a reconstruction of past climate that is consistent with proxies. The complete description of the experimental design including a brief description of the climate model, the experimental set-up, the data assimilation technique and the proxies selected for data assimilation is provided in Sect. 2. Section 3 investigates the impacts of a modification of atmospheric circulation and of WAIS fwf on SH surface climate and sea ice cover. Conclusions and perspectives are given in Sect. 4.

2 Experimental design

2.1 Model description

We have performed our experiments with the three-dimensional Earth climate model of intermediate complexity LOVECLIM. The model configuration includes a representation of atmosphere, ocean, sea ice and land surface. Each model component is briefly described here. A comprehensive description of the model is available in Goosse et al. (2010). The atmospheric component of LOVECLIM is ECBILT (Opsteegh et al., 1998). It is a quasi-geostrophic spectral model with 3 vertical levels corresponding to an equivalent horizontal resolution of $5.6 \times 5.6^{\circ}$ latitude-longitude. ECBILT is coupled with the ocean/sea ice model CLIO (Goosse and Fichefet, 1997; Fichefet and Morales Maqueda, 1997). CLIO is a general circulation model with a horizontal resolution of $3 \times 3^{\circ}$ and a vertical resolution ranging from 10 m near surface to 500 m at depth. LOVECLIM also contains the simple vegetation model VECODE (Brovkin et al., 2002) at the same resolution of the ECBILT model. Because LOVECLIM is much faster than many other three dimensional climate models, large ensembles of simulations can be carried out for data assimilation.

All experiments are driven by orbital forcing (Berger et al., 1978). Greenhouse gases concentrations are imposed from data of Flueckiger et al. (2002). As no ice sheet

Discussion Paper | Discussion Paper | Discussion Paper | Discussion Paper |

model is coupled to LOVECLIM in the configuration selected here, ice sheet topography and fwf are prescribed. The ice sheet topography from the reconstruction of Peltier et al. (2004) was adapted to LOVECLIM by Renssen et al. (2009). For the Laurentide ice sheet melting, fwf from Licciardi et al. (1999) is imposed for the St Lawrence and Hudson River outlets. It amounts to 40 mSv for both outlets at 10 ka and to 10 mSv and 70 mSv at 8 ka, respectively. In the experiments considered here, we have not prescribed additional fwf that could represent other sources, such as the melting of the Greenland and Scandinavian Ice sheets at 10 ka. For the Antarctic Ice Sheet fwf, we only consider a reference value for WAIS fwf prescribed at 50 mSv for both time slices based on Pollard and DeConto (2009). Additional experiments are performed using different fwf in the Southern Ocean (Table 2) as discussed in Sect. 3. This fwf is applied in Amundsen, Bellingshausen and West part of Weddell Seas. Melting of East Antarctic Ice Sheet is neglected (Mackintosh et al., 2011).

2.2 Assimilation method

The data assimilation method used here is the particle filter with re-sampling (van Leeuwen et al., 2009). A complete description of the procedure and the implementation is given in Dubinkina et al. (2011) but a brief summary is provided here. First, an ensemble of 48 simulations (called "particles" or ensemble members) is initialized by adding a small noise to the atmospheric stream function of a single model state. Each particle is then propagated in time by the climate model. After one year, the likelihood of each particle is computed from the difference between the observed or reconstructed temperatures and the simulated ones. The particles are then resampled according to their likelihood, i.e. to their ability to reproduce the signal derived from the available records. The particles with low likelihood are stopped, while the particles with a high likelihood are copied a number of times proportional to their likelihood in order to keep the total number of particles constant throughout the period covered by the simulations, keeping the new weight of each particle equal to one. A small noise is again added to the atmospheric stream function of each copy to obtain different time developments for

the following year. The entire procedure is repeated sequentially every year until the final year of calculation (400 yr here).

2.3 Proxy data

Temperature reconstructions used to constrain model results in the data assimilation experiments come from different archives. For marine and pollen records (Table 1, Fig. 1), original calibration is retained and the data error is assumed to be 0.7 °C. For ice cores (Table 1, Fig. 1, the data are based on δ^{18}O and δD measurements, scaled to temperature using the classical approach based on the spatial slope of 0.8 ‰/°C and 6.34 ‰/°C for δ^{18}O/T and δD/T, respectively (Masson-Delmotte et al., 2008). The uncertainty on temperature estimates remain difficult to fully quantify. Water stable isotope records in ice cores are affected by condensation temperature during precipitation events, but also by changes in ice sheet surface elevation (Siddall et al., 2012). While they are classically related to annual mean surface air temperature, these records are affected by precipitation intermittency (Laepple et al., 2011), boundary layer dynamics affecting the relationship between surface and condensation temperature, wind erosion and bychanges in moisture sources (Masson-Delmotte et al., 2011). These processes may produce a temporal isotope-temperature relationship which can be lower than the spatial gradient (Sime et al., 2008). Using the spatial gradient may therefore lead to an underestimation of temperature changes. As uncertainties on central East Antarctic temperature anomalies were suggested to reach 20–30 % (Jouzel et al., 2003), we decided to attribute an uncertainty on 10 and 8 ka anomalies of 0.3 °C. This small error bar is deliberately selected to strongly constrain on the simulations with data assimilation. A reasonable increase of the errors would not change qualitatively our conclusions but could modulate the amplitude of the simulated changes (Goosse et al., 2012).

In the data assimilation experiments, it is necessary to compare model results and data are through anomalies with respect to the reference period covering years from 1.5 to 0.5 ka. As a consequence, proxy records which do not cover both this reference period and the study period (from 8.5 to 7.5 ka for the snapshot at 8 ka or from 10.5 to

9.5 ka for the snapshot at 10 ka, respectively) with high enough temporal resolution (at least 300 yr) are excluded from our simulations with data assimilation. All the selected data are summarized in Table 1a. Some records rejected for data assimilation are kept for validation. The location of each record is shown in Fig. 1. We have also excluded the records from Byrd, Siple Dome, Plateau Remote and Dominion Range ice cores. The first ones (Byrd and Siple Dome records) may be affected by ice flow dynamics and quite strong variability in elevation (Sidall et al., 2012). The last ones (Plateau Remote and Dominion Range) present a too strong sampling variability (Masson-Delmotte et al., 2000).

These conditions of data selection do not allow keeping any data near the Kerguelen plateau, along the South America, the East Pacific and the West Atlantic and the West Antarctica. Therefore the data assimilation system constrains the model over the southern ocean with only 3 records (West Antarctic Peninsula, East Atlantic and Tasmania/New Zealand areas).

2.4 Simulation strategy

Several 400-yr-long equilibrium runs with constant forcing are realized for 10 and 8 ka with and without data assimilation. These simulations are initialized by results from a long equilibrium run (with a duration of 3000 yr) with constant forcings for 10 and 8 ka. They all include an ensemble of 48 particles. The simulations without data assimilation, named respectively STD8 and STD10, allow evaluating by comparison the impact of data assimilation. Hereafter, the simulated temperature refers to the mean state of the ensemble. Hereafter, the acronym STD corresponds to the difference between the snapshot simulations (STD8-STD10).

The control simulation used to compute the model anomalies and to compare them with proxy data anomalies in the data assimilation process, is based on a transient simulation carried out over the period 1–2000 CE. For the period 1–850 CE, no volcanic forcing is applied and total solar irradiance and land use change are derived from a linear interpolation between 1 and the value in 850 CE provided in the framework

of Paleo Modelling Intercomparison Project Phase 3 (PMIP3, Schmidt et al., 2011). Afterward, all the used forcings come from the PMIP3 protocol. The description of these forcings is detailed in Crespin et al. (2012).

First, to test the influence of changes in atmospheric circulation (first hypothesis), we performed simulations with assimilation of atmospheric and sea surface temperature data for both 10 and 8 ka (ATM10 and ATM8, Table 2). In these experiments, the atmospheric stream function is perturbed and the assimilation step (i.e. the selection of the ensemble members based on model-data comparison) is done each year. No modification of the fwf reference is applied in ATM8 and ATM10. When we discuss differences between these new simulations (ATM8-ATM10), the acronym ATM is used for simplicity.

The goal of the second group of experiments with data assimilation is to test the influence of changes in ocean temperatures. This is done by changing the fwf due to the WAIS melting between 10 and 8 ka. The "best guess" fwf for LOVECLIM is estimated using data assimilation. Here the assimilation time step is 50 yr as the response time of the ocean is much longer than of the atmosphere. A longer period is thus required to estimate the effect of the perturbation. The perturbed fwf applied at time t, FWF(t), is derived from an autoregressive process such as:

$$\mathrm{FWF}(t) = \mathrm{FWF}(t-1) + 0.5\,\epsilon_{\mathrm{FWF}}(t-1) + \epsilon_{\mathrm{FWF}})(t),$$

where $\epsilon_{\mathrm{FWF}}(t)$ is a Gaussian noise following the distribution $\mathcal{N}(0,\ \sigma_{\mathrm{FWF}})$. σ_{FWF} is equal to 30 mSv in this study. This method allows to extract a fwf that provides the best agreement with the proxy records. This method is applied in simulations named varFWF8 and varFWF10.

Third, two simulations without data assimilation are then carried out with the fwf estimates derived from varFWF8 and varFWF10 for 8 and 10 ka, respectively. These experiments are named FWF8 and FWF10.

Finally, in order to combine the effects of changes in atmospheric circulation and of an increase of fwf, additional experiments are performed with an atmospheric circulation perturbation and an assimilation time step of one year as for ATM8 and ATM10, and the fwf derived from varFWF8 and varFWF10. These experiments for 8 and 10 ka are named ATMFWF8 and ATMFWF10, respectively. This two step procedure is required as the current version of the data assimilation method is not adapted to handle processes characterized by very different time scales. All the simulations, their names, the type of perturbation and the amount of the fwf are described in Table 2. When we discuss the differences (FWF8-FWF10) and (ATMFWF8-ATMFWF10), the acronyms FWF and ATMFWF are used for simplicity.

For comparing model results with data, we use a root mean square error (RMSE) metrics:

$$\text{RMSE} = \sqrt{\overline{(\Delta T_{\text{mod}} - \Delta T_{\text{obs}})^2}},$$

where ΔT is the temperature differences between 8 and 10 ka. ΔT_{obs} (ΔT_{mod}) corresponds to temperature difference observed (modelised) at one location. The overbar denotes an average over all the Antarctic or the Southern Ocean data locations.

2.5 WAIS fresh water flux

In contrast to the NH, where the fwf due to ice sheet melting are relatively well documented (Licciardi et al., 1999), the Southern Hemisphere fwf and locations are not well known. There is no consensus between ice sheet modeling and marine δ^{18}O records.

From ice sheet modelling, Pollard et DeConto et al. (2009) diagnosed an amount of 50 mSv for the WAIS melting during the early Holocene (10 to 6 ka). This flux is the one apply in STD simulations. Earlier ice sheet reconstruction (Peltier, 2004) showed a larger melting rate of Antarctic ice sheet in 8 ka compared to 6 and 10 ka periods. Recent simulations of Mackintosh et al. (2011) exhibit a relatively constant melting rate between 11 and 7 ka followed by a weaker melting of the Antarctic ice sheet. While these modeling studies converge on a decrease of the melting rate around 6 ka, they diverge on the evolution of melting rate between 10 and 7 ka. Differences between

those studies could be explain by differences in forcing methods. All these studies are constrained by different and crude forcings for both atmospheric and oceanic components. The first study is driven by stacked deep-sea-core δ^{18}O record for the oceanic forcing and by a parameterization depending from elevation, orbital configuration and sea level. The reconstruction from Peltier (2004) is constrained by sea level curve and isostasy. The last study, is driven by modern temperature and precipitation climatology adjusted to follow the Vostok ice core record and forced also by oceanic heat flux driven mainly by changes in far-field ocean temperatures represented by a benthic δ^{18}O stack. Additionally, Pollard et DeConto (2009) show that ice sheet could be very sensitive to these forcings (especially the ocean heat fluxes).

For the WAIS, large regional differences are reported from glaciological studies. A gradually retreat of ice streams of Marie Byrd Land has been suggested (Stone et al., 2003). By contrast, a rapid retreat of the grounding line of the ice stream occupying the George VI Sound is documented around 9.5 ka, followed by stabilization of the ice stream (Bentley et al., 2010). On the other side of Antarctic Peninsula, the Larsen B persisted during the Holocene until its recent collapse (Domack et al., 2005). These examples show that the early Holocene history of the WAIS is complex and not sufficiently documented to build a common scenario. Furthermore, the melting rate of an ice shelf is influenced by the bathymetry profile below the ice shelf (Schoof et al., 2007). This point shows that non-climatic variables could also have a large impact on the location and the timing of ice shelf melting.

Marine observations from foraminifera and diatoms, which could be interpreted as indicators of the amount of fresh water release to the Southern Ocean (Bianchi et al., 2004), do not show drastic changes in the glacial meltwater inflow between 10 and 8 ka. In the south Atlantic (50–53° S, 5° E), the δ^{18}O measured in planktic foraminifers demonstrated a small trend toward lighter values between 9 and 7 ka (Bianchi et al., 2004). Similarly, the δ^{18}O measured in diatoms evidenced a 1.5 ‰ decrease over the course of the Holocene, with a small drop during the 10 to 8 ka BP period (Hodell et al., 2001). In coastal areas, a δ^{18}O diatom record from West Antarctic Peninsula presents a large drop between 10.5 and 8.9 ka BP while δ^{18}O diatom records in East Antarctica depicts a 500 yr event of light values centered at 9.2 ka BP (Crespin et al., 2012) or a small increase toward enriched values (Berg et al., 2010).

It is therefore difficult to faithfully assess changes in fwf due to WAIS melting between 10 and 8 ka from the existing data. The uncertainties on timing and melting rate are large enough to study here how modifications of this flux affect early Holocene SH high latitude climate.

3 Results

Running LOVECLIM without data assimilation (STD8 and STD10) does not reproduce the cooling observed at high southern latitude between 10 to 8 ka in both atmospheric and sea surface temperature. By contrast, the model simulates a warming between the two snapshots (Fig. 2a) especially south of the polar front (up to 0.5 °C). The comparison with proxy reconstruction available during these periods shows a relative high RMSE of 1.01 °C (Antarctica) and 1.28 °C (Southern Ocean) (Table 3).

This warming is caused by an inflow of warmer North Atlantic Deep Water (NADW) in the Southern Ocean at 8 ka compared to 10 ka. In both snapshots, the NH fwf is high enough to suppress the convection in the Labrador Sea. By contrast, the convection in Norwegian and Greenland Seas is active for both periods. As the Laurentide ice sheet is smaller at 8 ka than at 10 ka, the North Atlantic surface temperature is warmer. As explained in Renssen et al. (2010), the NADW formed in the Greenland and Norwegian Seas is then warmer inducing a warming at high southern latitude at 8 ka. As in Renssen et al. (2010) we call, hereafter, this processes an advective teleconnection.

The climate simulated in STD experiments is thus not consistent with data. This might be due to inadequate model physics that prevent a correct response to the forcing or to the experiment design, for instance a wrong choice of fwf.

Between ATM8 and ATM10, the changes in atmospheric circulation due to data assimilation imply a cooling over Antarctica and coastal areas in Bellingshausen Sea

and off Dronning Maud Land and Adélie Land (Fig. 2b). In contrast with STD that displays very weak changes in atmospheric circulation, the surface temperature changes simulated by the LOVECLIM model in ATM is due to a weakening of the Circum Polar Trough, especially in Ross Sea, Prydz Bay and Weddell Sea areas (Fig. 3b). The atmospheric circulation simulated in ATM8 restrains the inflow of warm air into the Antarctic area and limits also the outflow of cold air out of Antarctica. Consequently, this change in meridional atmospheric circulation leads to a cooling of the Antarctic continent. Even if the magnitude of the cooling (Fig. 2b) is weaker than in the reconstructions (Fig. 1), the simulated surface temperature field over Antarctica matches relatively well the observations (RMSE is 0.45 °C in ATM, Table 3). However, a warming is still simulated over the Southern Ocean, leading to larger errors (RMSE of 1.05 °C, Table 3). This warming is slightly reduced compared to the STD experiments (error of 1.28 °C in STD, Table 3), but cannot compensate for the upwelling of warmer CDW due to the advective tele-connection at 8 ka. To explain the observed cooling over Southern Ocean seen in the proxy-based temperature reconstructions at 8 ka, another mechanism has to be involved.

In the FWF experiments, we emulate the oceanic cooling by an increase of the fwf input. In this way, data assimilation experiment varFWF has been used to select the amount of fresh water release by the WAIS which best fits the surface temperature data at 10 and 8 ka (Fig. 4). At 10 ka, the fwf reconstructed by data assimilation is systematically lower than 50 mSv (variations between 10 and 50 mSv). The mean value is estimated to be 25 mSv instead of 50 mSv for the reference scenario used in STD10 (Fig. 4a). For the 8 ka period, the fwf estimates reaches an equilibrium after 100 yr. The selected scenario (120 mSv) suggests a larger WAIS melting (+140 %) than the reference one (Fig. 4b). Additional experiments carried out with assimilation of ice core data only (not shown) bring out almost the same scenarios for both period (50 mSv for 10 ka and 110 mSv for 8 ka). WAIS fwf calculated from simulation varFWF8 and varFWF10 represent our current "best guess" estimate. To explain the cooling in the Southern high latitudes during the transition between 10 to 8 ky BP, the data assimilation method suggests thus an increase of WAIS melting (~ 100 mSv in 8 ky BP compared to 10 ky BP). These fwf estimates are applied in the simulation FWF8 and FWF10. An increase of fwf during this cold event could be counter intuitive. However, melting of the ice sheet is not a simple direct response of the surface forcing and the ice sheet responds slowly to climate change (Bentley et al., 2010). Thus a long lag between the warm period observed at 10 ka and the melting of the ice sheets could occur. In addition, ocean processes linked to a release of fresh water leads to a warming of subsurface water masses (below 100m) south of 60° S (Swingedouw et al., 2009). A similar subsurface warming has been simulated in northern high latitude during large melting events (Flueckiger et al., 2006). This could create a positive feed back by increasing the ice shelves melting. Therefore, due to nonlinear response to ice sheet and oceanic feedback, a larger fwf melting during a cold event is a reasonable scenario. Furthermore, as summarized in Sect. 2.5, no observations can be used to support or refute the magnitude and sign of these changes. We therefore consider our results as a rough, first order estimate of fwf amounts (which could be model dependent) but not as a precise fwf reconstructions.

As expected, in FWF simulations, a large cooling (up to −2 °C between STF and ASF) is simulated over most of the Southern Ocean from 10 to 8 ka. However, this only produces a slight Antarctic cooling (Fig. 2c). The obtained surface temperature pattern matches well the Southern Ocean proxy, leading to a RMSE of 0.73 °C, which is better than the one observed in ATM and STD (Table 3). However, over the interior Antarctica, the ice core data suggest a much larger cooling than the one simulated in FWF experiments (RMSE of 0.74 °C). A consequence of this large Southern Ocean cooling is a deepening of the Circumpolar Trough and an increase of the SWW (+6 %) (Fig. 3c). This strengthening of the Westerlies (below 50° S) at 8 ka fits the reconstruction of SWW strength performed by McGlone et al. (2011). However, over the Antarctic Peninsula, Shevenell et al. (2012) suggest a decrease of the SWW strength which is not simulated in FWF.

The ocean and the atmosphere circulation changes have thus complementary effects on the surface temperature. The first one leads to a relatively large cooling over the Southern Ocean that is absent in the AMS-experiments, and the second one leads to large cooling over the Antarctic continent. Therefore, to decrease both Southern Ocean and Antarctic continent surface temperature as shown in the observations (Fig. 1), one solution is to associate the method used for the ATM simulations with the fwf applied in FWF simulations. When both ATM and FWF are combined (in ATMFWF), the simulations produce a large cooling over the SO (about −1.6 °C) and a slightly larger cooling over the Antarctic continent (about −0.6 °C) compared to STD. This cooling is also larger in Antarctica than the one simulated in ATM alone as shown in Fig. 2d during the transition from 10 to 8 ka BP. The corresponding minimum errors are 0.38 °C for the Antarctic proxy data and 0.61 °C for the Southern Ocean data (Table 3). The comparison of the different panels in Fig. 3 highlights that the response of the atmospheric dynamics to the data assimilation in the ATMFWF is roughly the sum of the changes seen in ATM and in FWF.

Data assimilation in ATM, FWF and ATMFWF does not only modify the annual mean state but also the seasonal cycle at all southern latitudes (Fig. 5). In the reference simulation, in central Antarctica (south of 75° S), insolation changes between 10 and 8 ka induce a winter cooling (from March to October) and a summer warming (from November to February), with a lag of one month as noticed in previous studies (Crucifix et al., 2002; Renssen et al., 2005). For oceanic regions (between 75° S to 55° S), 8 ka snapshot is warmer than the 10 ka snapshot during all the year. The seasonal timing of the largest warming simulated in STD depends on the latitude. The largest warming occurs from November to January at 75° S and from July to August at 55° S (Fig. 5).

In FWF (and ATMFWF), the stratification of surface ocean layer is strongest due to the larger release of fresh water at 8 ka and consequently vertical transport of heat is reduced. In FWF, the atmosphere is cooled in winter by −0.3 °C. During summer time (November to February), a weak warming is simulated (about 0.6 °C) between 10 and 8 ka. This feature is very similar to the one modelised in STD. By contrast, over the ocean (north of 70° S), the atmosphere is cooled during almost all the year in FWF. In FWF, the period characterized by the largest vertical heat exchanges in the ocean in STD simulation (May to September) is characterized by the coldest period in FWF (more than 1.5 °C cooling) (Fig. 5).

In ATM (and ATMFWF), the atmospheric circulation reconstruction induces an enhanced seasonal cycle over the Antarctic continent with similar summer and cooler winter compared to STD and FWF, respectively. Compared to STD and FWF, the change of atmospheric circulation obtained by data assimilation and its impact on surface temperature is almost the same in ATM and FWFATM. From 10 to 8 ka, the atmospheric circulation changes constrained by surface temperature data induce a cooling of −0.5 (−0.3) °C over Antarctica during winter in ATM (ATMFWF) and −0.2 (−0.1) °C over the Southern Ocean during all the year, compared to the transition in STD (FWF) (Fig. 5e and f).

Between 55° S and 40° S, the seasonal and interannual variabilities of the surface temperature in the ACC are weak in STD, ATM, FWF and ATMFWF. Modifications of fwf or of the atmospheric circulation only alter the annual mean temperature without changing the amplitude of the seasonal cycle, only the annual temperature is modified.

The changes in surface air temperature due to modifications in atmospheric circulation or due to the cooling of oceanic surface temperatures are associated with an increase in sea ice concentration and sea ice duration (Fig. 6), two variables for which proxy information is available. Reconstructions display an increase of sea ice duration from 10 to 8 ka off the East Antarctic coast (Crosta et al., 2008; Denis et al., 2009; Verkulish et al., 2002) and a congruent northward migration of the sea-ice front from ∼ 55° S to ∼ 53° S in the Antarctic Atlantic (Bianchi and Gersonde, 2004; Nielsen et al., 2004).

In each simulation driven by surface temperature data assimilation, sea ice is present all year long in the southern part of Weddell and Ross Sea. Consequently, no change is visible in sea ice duration there. The seasonal sea ice cover has different behavior if a cooling and a freshening of the oceanic surface is applied or not. In the STD, a

decrease of sea-ice duration by 10 days is simulated together with a lower maximum and minimum sea ice extent (−0.5 million km^2) (Fig. 6a). In the ATM simulation, the atmospheric circulation selected by the particle filter leads to an increase of sea ice duration off West Coast of Antarctic Peninsula, Dronning Maud Land and Wilkes Land (Fig. 6b). This is in agreement with the simulated temperature patterns (Fig. 2b and d). In FWF and ATMFWF simulations, the cooling and freshening of ocean surface from 10 to 8 ka conduct to an increase of sea ice duration by two months, an increase of winter sea ice extent by 2.5 million km^2 and a northward migration of the sea-ice front in the Atlantic sector (Fig. 6c and d). However, in some grid points close to Dronning Maud Land, sea ice cover duration is reduced in FWF (Fig. 6c). This is due to warmer summer conditions (not shown here) and advection of warmer air mass, coming from the north, in this area.

The sea ice simulated in FWF and ATMFWF is thus in good qualitative agreement with published proxy records. This suggests that sea ice changes are mainly driven by the oceanic cooling (second hypothesis) rather than by modifications of the atmospheric circulation (first hypothesis) during this period.

4 Conclusions

We have presented simulations performed with an intermediate complexity climate model, including experiments with data assimilation, to study the mechanisms responsible for the reconstructed southern high latitude cooling from 10 to 8 ka. We have tested two hypotheses, without taking into account other factors such as changes in the Antarctic ice sheet topography, or changes in ice shelves. Our data assimilation methodology is not yet able to deal directly with processes with very different timescales (atmospheric and oceanic ones). We therefore evaluated their contributions in separate experiments. The good agreement between our final set of simulations (ATMFWF) and proxy data is encouraging. Further limitations of our approach lie in the uncertainties on the Greenland and Laurentide ice sheet melting. In particular, Licciardi et al. (1999) show that their input into Arctic Ocean is about 11 mSv at 10 ka, which represents 12 % of the total water injected at 10 ka in STD. Clark et al. (2012) report large changes of the Scandinavian Ice Sheet area between 11 and 10 ka. These sources of melt water in Northern Hemisphere which are not incorporated in our set of simulations could further modulate the intensity of bottom water formation in the Norwegian and Greenland Seas (Bakker et al., 2012) and affect inter hemispheric tele-connections mechanism (bi-polar seesaw and advective tele-connection).

Northern hemisphere data assimilation may help to constrain those inputs as well as the characteristics of deep water formed in the North Atlantic, with a potential impact on CDW and thus on the southern ocean surface temperature. However, in our current experimental setup, we cannot modify the presence of warmer CDW at 8 ka compared to 10 ka. This is due to the lack of data assimilation in the NH, which are difficult to take into account in data assimilation due to their long time scales.

Despite those limitations, the results presented here provide a consistent picture of the climate change from 10 to 8 ka, for the continent and Southern Ocean. Our study suggests the following results:

- Inter-hemispheric oceanic tele-connections (active in both snapshots) and warmer NH high latitude climate at 8 ka, leads to warmer CDW and warmer surface temperatures in Southern Ocean and over Antarctica at 8 ka compared to 10 ka. This means that the standard model configuration cannot simulate the observed cooling at SH high latitudes (with the exception of winter changes).

- Our data assimilation experiments show that the cooling over the Antarctic continent can be explained by a change in the atmospheric circulation and a modification of the meridional heat transport in the coastal areas. The Southern Ocean cooling is mainly driven by an increase of the fresh water release from the WAIS (+100 mSv). This hypothesis is in agreement with model physics and surface temperature reconstructions. So far, no evidence from ice sheet modeling or glaciological reconstructions of can support or invalidate this hypothesis.

- Consequences of the oceanic cooling on sea ice are compatible with the increase of the simulated sea ice duration observed in coastal region of East Antarctica and in the Atlantic sector.

Acknowledgements. We acknowledge D. Roche for making available the ice sheet forcing data for the LOVECLIM model. H. Goosse is Senior Research Associate with the Fonds National de la Recherche Scientifique (F.R.S. – FNRS-Belgium). P. Mathiot is Postdoctoral researcher with F.R.S. – FNRS-Belgium. This work has been performed in the framework of the ESF HOLOCLIP project (a joint research project of the European Science Foundation PolarCLIMATE program, is funded by national contributions from Italy, France, Germany, Spain, The Netherlands, Belgium and the UK), by the Belgian Federal Science Policy Office (Research Program on Science for a Sustainable Development) and is also supported by F.R.S. – FNRS. The research leading to these results has received funding from the European Union's Seventh Framework programme (FP7/2007-2013) under grant agreement no. 243908, "Past4Future. Climate change – Learning from the past climate"... Computational resources have been provided by the supercomputing facilities of the Université catholique de Louvain (CISM/UCL) and the Consortium des Equipements de Calcul Intensif en Fédération Wallonie Bruxelles (CECI) funded by FRS-FNRS. This is HOLOCLIP contribution XX and Past4future contribution XX.

References

Bakker, P., Van Meerbeeck, C. J., and Renssen, H.: Sensitivity of the North Atlantic climate to Greenland Ice Sheet melting during the Last Interglacial, Clim. Past, 8, 995–1009, doi:10.5194/cp-8-995-2012, 2012.

Barbara, L., Crosta, X., Massé, G., and Ther, O.: Deglacial environments in eastern Prydz Bay, East Antarctica, Quaternary Sci. Rev., 29, 2731–2740, 2010.

Barrow, T. T., Lehman, S. J., Fifield, L. K., and De Deckker, P.: Absence of cooling in New Zealand and the adjacent ocean during the younger dryaschronozone, Science, 318, 86–89, 2007.

Bentley, M. J.: The Antarctic paleo record and its role in improving predictions of future Antarctic Ice Sheet change, J. Quaternary Sci., 25, 5–18, 2010.

Berger, A. L.: Long-term variations of daily insolation and Quaternary climatic changes, J. Atmos. Sci., 35, 2363–2367, 1978.

Bianchi, C. and Gersonde, R.: Climate evolution at the last deglaciation: the role of the Southern Ocean, Earth Planet. Sc. Lett., 228, 407–424, 2004.
Boës, X. and Fagel, N.: Relationships between southern Chilean varved lake sediments, precipitation and ENSO for the last 600 years, J. Paleolimnol., 39, 237–252, 2008.
Brook, E. J., White, J. W. C., Schilla, A. S. M., Bender, M. L., Barnett, B., Severinghaus, J. P., Taylor, K. C., Alley, R. B., and Steig, E. J.: Timing of millennial-scale climate change at Siple Dome, West Antarctica, during the last glacial period, Quaternary Sci. Rev., 24, 1333–1344, 2005.
Brovkin, V., Bendtsen, J., Claussen, M., Ganopolski, A., Kubatzki, C., Petoukhov, V., and Andreev, A.: Carbon cycle, vegetation and climate dynamics in the Holocene: experiments with the CLIMBER-2 model, Global Biogeochem. Cy., 16, 1139, doi:10.1029/2001GB001662, 2002.
Clark, P. U., Shakun, J. D., Baker, P. A., Bartlein Simon Brewer, P. J., Brook, E., Carlson, A. E., Cheng, H., Kaufman, D. S., Liu, Z., Marchitto, T. M., Mix, A. C., Morrill, C., Otto-Bliesner, B. L., Pahnke, K., Russell, J. M., Whitlock, C., Adkins, J. F., Blois, J. L., Clark, J., Colman, S. M., Curry, W. B., Flower, B. P., He, F., Johnson, T. C., Lynch-Stieglitz, J., Markgraf, V., McManus, J., Mitrovica, J. X., Moreno, P. I., and Williams, J. W. : Global climate evolution during the last deglaciation, P. Natl. Acad. Sci., 109, E1134–E1142, 2012.
Cook, E. R., Buckley, B. M., D'Arrigo, R. D., and Peterson, M. J.: Warm-season temperatures since 1600 BC reconstructed from Tasmanian tree rings and their relationship to large-scale sea surface temperature anomalies, Clim. Dynam., 16, 79–91, 2000.
Cook, E. R., Buckley, B. M., Palmer, J. G., Fenwick, P., Peterson, M. J., Boswijk, G., and Fowler, A.: Millennia-long tree-ring records from Tasmania and New Zealand: a basis for modelling climate variability and forcing, past, present and future, J. Quaternary Sci., 21, 689–699, 2006.
Cortese, G., Abelmann, A., and Gersonde, R.: The last five glacial-interglacial transitions: A high-resolution 450,000-year record from the subantarctic Atlantic, Paleoceanography, 22, PA4203, doi:10.1029/2007PA001457, 2007.
Crespin, E., Goosse, H., Fichefet, T., Mairesse, A., and Sallaz-Damaz, Y.: Arctic climate over the past millennium: annual and seasonal responses to external forcings, Holocene, doi:10.1177/0959683612463095, in press, 2012.

Crespin, J., Yam, R., Crosta, X., Massé, G., Schmidt, S., Campagne, P., and Shemesh, A.: East Antarctic Holocene glaciers fluctuations and unprecedented recent instability, Nat. Geosci., submitted, 2012.
Crosta, X., Sturm, A., Armand, L., and Pichon, J.-J.: Late Quaternary sea ice history in the Indian sector of the Southern Ocean as recorded by diatom assemblages, Mar. Micropaleontol., 50, 209–223, doi:10.1016/S0377-8398(03)00072-0, 2004.
Crosta, X., Crespin, J., Billy, I., and Ther, O.: Major factors controlling Holocene δ^{13}C_org changes in a seasonal sea ice environment, Adélie Land, East Antarctica, Global Biogeochem. Cy., 19, GB4029, doi:10.1029/2004GB002426, 2005.
Crosta, X., Denis, D., and Ther, O.: Sea ice seasonality during the Holocene, Adélie Land, East Antarctica, Mar. Micropaleontol., 66, 222–232, doi:10.1016/j.marmicro.2007.10.001, 2008.
Crowley, T. J.: North Atlantic Deep Water cools the Southern Hemisphere, Paleoceanography, 7, 489–497, 1992.
Denis, D., Crosta, X., Schmidt, S., Carson, D., Ganeshram, R., Renssen, H., Bout-Roumazeilles, V., Zaragosi, S., Martin, B., Cremer, M., and Giraudeau, J.: Holocene glacier and deep water dynamics, Adélie Land region, East Antarctica, Quaternary Sci. Rev., 28, 1291–1303, 2009.
Denis, D., Crosta, X., Barbara, L., Masse, G., Renssen, H., Ther, O., and Giraudeau, J.: Sea ice and wind variability during the Holocene in East Antarctica: insight on middle–high latitude coupling, Quaternary Sci. Rev., 29, 3709–3719, 2010.
Domack, E., Duran, D., Leventer, A., Ishman, S., Doane, S., McCallum, S., Amblas, D., Ring, J., Gilbert, R., and Prentice, M.: Stability of the Larsen B ice shelf on the Antarctic Peninsula during the Holocene epoch, Nature, 436, 681–684, 2005.
Dubinkina, S., Goosse, H., Damas-Sallaz, Y., Crespin, E., and Crucifix, M.: Testing a particle filter to reconstruct climate changes over the past centuries, Int. J. Bifurcat. Chaos, 21, 3611, doi:10.1142/S0218127411030763, 2011.
EPICA-community-members: One-to-one coupling of glacial climate variability in Greenland and Antarctica, Nature, 444, 195–198, 2006.
Farmer, E. C., deMenocal, P. B., and Marchitto, T. M.: Holocene and deglacial ocean temperature variability in the Benguela upwelling region: implications for law-latitude atmospheric circulation, Paleoceanography, 20, PA2018, doi:10.1029/2004PA001049, 2005.

Discussion Paper | Discussion Paper | Discussion Paper | Discussion Paper |

Fletcher, M.-S. and Moreno, P. I.: Have the Southern Westerlies changed in a zonally symmetric manner over the last 14,000 years? A hemisphere-wide take on a controversial problem, Quatern. Int., 253, 32–46, 2012.

Flückiger, J., Monnin, E., Stauffer, B., Schwander, J., Stocker, T. F., Chappellaz, J., Raynaud, D., and Barnola, J.-M.: High resolution Holocene N_2O ice core record and its relationship with CH_4 and CO_2, Global Biogeochem. Cy., 16, 1010, doi:10.1029/2001GB001417, 2002.

Goosse, H., Lefebvre, W., de Montety, A., Crespin, E., and Orsi, A. H.: Consistent past half-century trends in the atmosphere, the sea ice and the ocean at high southern latitudes, Clim. Dynam., 33, 999–1016, 2009.

Goosse, H., Brovkin, V., Fichefet, T., Haarsma, R., Huybrechts, P., Jongma, J., Mouchet, A., Selten, F., Barriat, P.-Y., Campin, J.-M., Deleersnijder, E., Driesschaert, E., Goelzer, H., Janssens, I., Loutre, M.-F., Morales Maqueda, M. A., Opsteegh, T., Mathieu, P.-P., Munhoven, G., Pettersson, E. J., Renssen, H., Roche, D. M., Schaeffer, M., Tartinville, B., Timmermann, A., and Weber, S. L.: Description of the Earth system model of intermediate complexity LOVECLIM version 1.2, Geosci. Model Dev., 3, 603–633, doi:10.5194/gmd-3-603-2010, 2010.

Goosse, H., Crespin, E., Dubinkina, S., Loutre, M. F., Mann, M. E., Renssen, H., Sallaz-Damaz, Y., and Shindell, D.: The role of forcing and internal dynamics in explaining the “Medieval Climate Anomaly”, Clim. Dynam., doi:10.1007/s00382-012-1297-085, in press, 2012.

Hodell, D. A., Kanfoush, S. L., Shemesh, A., Crosta, X., Charles, C. D., and Guilderson, T. P.: Abrupt cooling of Antarctic surface waters and sea ice expansion in the South Atlantic Sector of the Southern Ocean at 5000 cal yr B.P., Quaternary Res., 56, 191–198, 2001.

Holden, P. B., Edwards, N. R., Wolff, E. W., Lang, N. J., Singarayer, J. S., Valdes, P. J., and Stocker, T. F.: Interhemispheric coupling, the West Antarctic Ice Sheet and warm Antarctic interglacials, Clim. Past, 6, 431–443, doi:10.5194/cp-6-431-2010, 2010.

Kaiser, J., Lamy, F., and Hebbeln, D.: A 70-kyr sea surface temperature record off southern Chile (Ocean Drilling Program Site 1233), Paleoceanography, 20, PA4009, doi:10.1029/2005PA001146, 2005.

Katsuki, K., Ikehara, M., Yokoyama, Y., Yamane, M., and Khim, B.-K.: Holocene migration of oceanic front systems over the Conrad Rise in the Indian Sector of the Southern Ocean, J. Quaternary Sci., 27, 203–210, 2012.

Kim, J. H., Schneider, R. R., Hebbeln, D., Muller, P. J., and Wefer, G.: Last deglacial sea-surface temperature evolution in the Southeast Pacific compared to climate changes on the South American continent, Quaternary Sci. Rev., 21, 2085–2097, 2002.

Kim, J. H., Schouten, S., Hopmans, E. C., Donner, B., and Sinninghe Damsté, S.: Global sediment core-top calibration of the TEX86 paleothermometer in the ocean, Geochim. Cosmochim. Acta, 72, 1154–1173, 2012.

Lamy, F., Ruhlemann, C., Hebbeln, D., and Wefer, G.: High- and low-latitude climate control on the position of the southern Peru-Chile Current during the Holocene, Paleoceanography, 17, 1028, doi:10.1029/2001PA000727, 2002.

Lamy, F., Kilian, R., Arz, H. W., François, J.-P., Kaiser, J., Prange, M., and Steinke, T.: Holocene changes in the position ant the intensity of the southern westerly wind belt, Nat. Geosci., 3, 695–699, doi:10.1038/NGEO959, 2010.

Licciardi, J. M., Teller, J. T., and Clark, P. U.: Freshwater Routing by the Laurentide Ice Sheet During the last Deglaciation, Mechanism of global Climate Change at Millennial Time Scales, Geophysical Monograph, 112, 1999.

Mackintosh, A., Golledge, N., Domack, E., Dunbar, R., Leventer, A., White, D., Pollard, D., DeConto, R., Fink, D., Zwartz, D., Gore, D. ,and Lavoie, C.: Retreat of the East Antarctic ice sheet during the last glacial termination, Nat. Geosci., 4, 195–202, doi:10.1038/NGEO1061, 2011.

Masson-Delmotte, V., Vimeux, F., Jouzel, J., Morgan, V., Delmotte, M., Ciais, P., Hammer, C., Johnsen, S., Lipenkov, V. Y., Mosley-Thompson, E., Petit, J.-R., Steig, E. J., Stievenard, M., and Vaikmae, R.: Holocene Climate Variability in Antarctica Based on 11 Ice-Core Isotopic Records, Quaternary Res., 54, 348–358, 2000.

Masson-Delmotte, V., Stenni, B., and Jouzel, J.: Common millennial-scale variability of Antarctic and Southern Ocean temperatures during the past 5000 years reconstructed from the EPICA Dome C ice core, Holocene, 14, 145–151, 2004.

Masson-Delmotte, V., Hou, S., Ekaykin, A., Jouzel, J., Aristarain, A., Bernardo, R. T., Bromwich, D., Cattani, O., Delmotte, M., Falourd, S., Frezzotti, M., Gallée, H., Genoni, L., Isaksson, E., Landais, A., Helsen, M. M., Hoffmann, G., Lopez, J., Morgan, V., Motoyama, H., Noone, D., Oerter, H., Petit, J. R., Royer, A., Uemura, R., Schmidt, G. A., Schlosser, E., Simões, J. C., Steig, E. J., Stenni, B., Stievenard, M., van den Broeke, M. R., van de Wal, R. S. W., van de Berg, W. J., Vimeux, F., and White, J. W. C.: A review of Antarctic surface snow isotopic

composition: observations, atmospheric circulation and isotopic modelling, J. Climate, 21, 3359–3387, 2008.
Masson-Delmotte, V., Stenni, B., Blunier, T., Cattani, O., Chappellaz, J., Cheng, H., Dreyfus, G., Edwards, R. L., Falourd, S., Govin, A., Kawamura, K., Johnsen, S. J., Jouzel, J., Landais, A., Lemieux-Dudon, B., Lourantou, A., Marshall, G., Minster, B., Mudelsee, M., Pol, K., Rothlisberger, R., Selmo, E., and Waelbroeck, C.: Abrupt change of Antarctic moisture origin at the end of Termination II, P. Natl. Acad. Sci., 107, 12091–12094, doi:10.1073/pnas.0914536107, 2010.
Masson-Delmotte, V., Buiron, D., Ekaykin, A., Frezzotti, M., Gallée, H., Jouzel, J., Krinner, G., Landais, A., Motoyama, H., Oerter, H., Pol, K., Pollard, D., Ritz, C., Schlosser, E., Sime, L. C., Sodemann, H., Stenni, B., Uemura, R., and Vimeux, F.: A comparison of the present and last interglacial periods in six Antarctic ice cores, Clim. Past, 7, 397–423, doi:10.5194/cp-7-397-2011, 2011.
McGlone, M. S., Turney, C. S. M., Wilmshurt, J. M., Renwick, R., and Pahnke, K.: Divergent trends in land and ocean temperature in the southern Ocean over the past 18,000 years, Nat. Geosci., 3, 622–626, 2010.
Mulvaney, R., Oerter, H., Peel, D. A., Graf, W., Arrowsmith, C., Pasteur, E. C., Knight, B. Littot, G. C., and Miners, W. D.: 1000-year ice core records from Berkner Island, Antarctic, Ann. Glaciol., 35, 45–51, 2002.
Nielsen, S. H. H., Koc, N., and Crosta, X.: Holocene climate in the Atlantic sector of the Southern Ocean: Controlled by insolation or oceanic circulation?, Geology, 32, 317–320, doi:10.1130/G20334.1, 2004.
Nikolaiev, V. I., Kotlyakov, V. M., and Smirnov, K. E.: Isotopic studies of the ice core from the Komsomolskaia station, Antarctica, Data of Glaciological Studies of the USSR Academy of Sciences, 63, 97–102, 1988.
Opsteegh, J. D., Haarsma, R. J., Selten, F. M., and Kattenberg, A.: ECBilt: A dynamic alternative to mixed boundary conditions in ocean models, Tellus A, 50, 348–367, 1998.
Pahnke, K. and Sach, P.: Sea surface temperature of southern midlatitudes 0–160 kyr BP, Paleoceanograpgy, 21, PA2003, doi:10.1029/2005PA001191, 2006.
Peltier, W. R.: Global glacial isostay and the surface of the ice-age earth: The ICE-5G (VM2) Model and GRACE, Annu. Rev. Earth Pl. Sci., 32, 111–149, doi:10.1146/annurev.earth.32.082503.144359, 2004.

Pichon, J.-J.: Les diatomées traceurs de l'évolution climatique et hydrologique de l'Océan Austral au cours du dernier cycle climatique. PhD. Thesis, Université Bordeaux 1, 279 pp., 1985.
Pollard, D. and DeConto, R. M.: Modelling West Antarctic ice sheet growth and collapse through the past five million years, Nature, 458, 329–332, 2009.
Renssen, H., Goosse, H., Fichefet, T., Masson-Delmotte, V., and Koc, N.: The Holocene climate evolution in the high-latitude Southern Hemisphere simulated by a coupled atmosphere-sea ice-ocean-vegetation model, Holocene, 15, 951–964, 2005.
Renssen, H., Seppä, H., Heiri, O., Roche, D. M., Goosse, H., and Fichefet, T.: The spatial and temporal complexity of the Holocene thermal maximum, Nat. Geosci., 2, 411–414, doi:10.1038/NGEO513, 2009.
Renssen, H., Goosse, H., Crosta, X., and Roche, D. M.: Early Holocene Laurentide Ice Sheet deglaciation causes cooling in the high-latitude Southern Hemisphere through oceanic teleconnection, Paleoceanography, 25, PA3204, doi:10.1029/2009PA001854, 2010.
Salvignac, M.-E.: Variabilité hydrologique et climatique dans l'Océan Austral (secteur indien) au cours du Quaternaire terminal, Essai de corrélations inter-hémisphériques, PhD. Thesis, Université Bordeaux 1, 308 pp., 1998.
Schmidt, G. A., Jungclaus, J. H., Ammann, C. M., Bard, E., Braconnot, P., Crowley, T. J., Delaygue, G., Joos, F., Krivova, N. A., Muscheler, R., Otto-Bliesner, B. L., Pongratz, J., Shindell, D. T., Solanki, S. K., Steinhilber, F., and Vieira, L. E. A.: Climate forcing reconstructions for use in PMIP simulations of the last millennium (v1.0), Geosci. Model Dev., 4, 33–45, doi:10.5194/gmd-4-33-2011, 2011.
Schoof, C.: Ice sheet grounding line dynamics: Steady states, stability, and hysteresis, J. Geophys. Res., 112, F03S28, doi:10.1029/2006JF000664, 2007.
Shevenell, A. E., Ingalls, A. E., Domack, E. W., and Kelly, C.: Holocene Southern Ocean surface temperature variability west of the Antarctic Peninsula, Nature, 470, 250–254, 2011.
Sicre, M. A., Labeyrie, L., Ezat, U., Duprat, J., Turon, J. L., Schmidt, S., Michel, E., and Mazaud, A.: Mid-latitude Southern Indian Ocean response to Northern Hemisphere Heinrich events, Earth Planet. Sc. Lett., 240, 724–731, 2005.
Sidall, M., Milne, G. A., and Masson-Delmotte, V.: Uncertainties in elevation changes and their impact on Antarctic temperature records since the end of the last glacial period, Earth Planet. Sc. Lett., 315–316, 12–23, 2012.

Sime, L. C., Tindall, J. C., Wolff, E. W., Connolley, W., and Valdes, P. J.: Antarctic isotopic thermometer during a CO_2 forced warming, J. Geophys. Res., 113, D24119, doi:10.1029/2008JD010395, 2008.
Steig, E., Brook, E. J., White, J. W. C., Sucher, C. M., Bender, M. L., Lehman, S. J., Morse, D. L., Waddigton, E. D., and Clow, G. D.: Synchronous climate changes in Antarctica and the North Atlantic, Science, 282, 92–95, 1998.
Stenni, B., Buiron, D., Frezzotti, M., Albani, S., Barbante, C., Bard, E., Barnola, J. M., Baroni, M., Baumgartner, M., Bonazza, M., Capron, E., Castellano, E., Chappellaz, J., Delmonte, B., Falourd, S., Genoni, L., Iacumin, P., Jouzel, J., Kipfstuhl, S., Landais, A., Lemieux-Dudon, B., Maggi, V., Masson-Delmotte, V., Mazzola, C., Minster, B., Montagnat, M., Mulvaney, R., Narcisi, B., Oerter, H., Parrenin, F., Petit, J. R., Ritz, C., Scarchilli, C., Schilt, H., Schüpbach, S., Schwander, J., Selmo, E., Severi, M., Stocker, T. F., and Udisti, R.: The expression of the bipolar climate seesaw around Antarctica during the last deglaciation, Nat. Geosci., 4, 46–49, 2011.
Stocker, T. F.: The seesaw effect, Science, 282, 61–62, 1998.
Stone, J. O., Balco, G. A., Sugden, D. E., Caffee, M. W., Sass, L. C., Cowdery, S. G., and Siddoway, C.: Holocene deglaciation of Marie Byrd Land, West Antarctica, Science, 299, 99–102, 2003.
Swingedouw, D., Fichefet, T., Goosse, H., and Loutre, M. F.: Impact of transient freshwater releases in the Southern Ocean on the AMOC and climate, Clim. Dynam., 33, 365–381, doi:10.1007/s00382-008-0496-1, 2009.
Van Leeuwen, P. J.: Particle filtering in Geophysical Systems, Mon. Weather Rev., 137, 4089–4114, 2009.
Verkulich, S. R., Melles, M., Hubberten, H.-W., and Pushina, Z. V.: Holocene environmental changes and evolution of Figurnoye Lake in the southern Bunger Hills, East Antarctica, J. Paleolimnol., 28, 253–267, 2002.
Vimeux, F., Masson, V., Jouzel, J., Stievenard, M., and Petit, J. R.: Glacial-interglacial changes in ocean surface conditions in the Southern Hemisphere, Nature, 398, 410–413, 1999.
Von Gunten, L. Grosjean, M., Rein, B., Urrutia, R., and Appleby, P.: A quantitative high resolution summer temperature reconstruction based on sedimentary pigments from Laguna Aculeo, Central Chile, back to AD 850, Holocene, 19, 873–881, 2009.

Watanabe, O., Jouzel, J., Johnsen, S., Parrenin, F., Shoji, H., and Yoshida, N.: Homogeneous climate variability across East Antarctica over the past three glacial cycles, Nature, 422, 509–512, 2003.
Xiong, L. and Palmer, J. G.: Reconstruction of New Zealand temperatures to AD 1720 using Libocedrubidwillii tree-rings, Climatic Change, 45, 339–359, 2000.

Discussion Paper | Discussion Paper | Discussion Paper | Discussion Paper |

Table 1. (a) Description of all the proxy records used in the data assimilation experiments. (b) Description of all the proxy records used for model validation. The classification of proxy records from the subtropical area or from the Southern Ocean (north of 66° S and south of subtropical front) depends on the type of climate dynamics suggested in the corresponding reference.

(a) Id	Name	Location	Proxy type	Reference
1	Law Dome	Antarctica	$\delta^{18}O$	Courtesy from T. van Ommen, Moy et al. (2012)
2	Vostok	Antarctica	$\delta^{18}O$	Vimeux et al. (1999)
3	Taylor Dome	Antarctica	$\delta^{18}O$	Steig et al. (1998)
4	Fuji Dome	Antarctica	$\delta^{18}O$	Watanabe et al. (2003)
5	EDC	Antarctica	$\delta^{18}O$	Masson-Delmotte et al. (2004)
6	KMS	Antarctica	δD	Nikolaiev et al. (1988)
7	TALDICE	Antarctica	$\delta^{18}O$	Stenni et al. (2010)
8	EDML	Antarctica	$\delta^{18}O$	EPICA Comm. Members (2006)
9	MtHoney	Southern Ocean	Pollen	McGlone et al. (2010)
10	TN057-17TC	Southern Ocean	Diatoms	Nielsen et al. (2004)
11	MD03-2611	Sub Tropical	Alkenone	Lamy et al. (2002)
12	ODP1084B	Sub Tropical	Mg/Ca	Farmer et al. (2005)
13	ODP 1098	Southern Ocean	TEX_{86}	Shevenell et al. (2011)

(b) Id	Name	Location	Proxy type	Reference
21	MD97-2121	Sub Tropical	Alkenone	Pahnke and Sachs (2006)
22	GIK17748-2	Sub Tropical	Alkenone	Kim et al. (2002)
23	IODP1089	Sub Tropical	Radiolerian	Cortese et al. (2007)
24	MD88-770	Sub Tropical	Foraminifera	Salvignac (1998)
25	MD97-2120	Southern Ocean	Alkenone	Pahnke and Sachs (2006)
26	IODP1233	Southern Ocean	Alkenone	Kaiser et al. (2005)
27	TNO57-13-PC4	Southern Ocean	Diatoms	Hodell et al. (2001)
28	MD97-2101	Southern Ocean	Diatoms	Crosta et al. (2005)
29	SO136-111	Southern Ocean	Diatoms	Crosta et al. (2004)
30	MD84-551	Southern Ocean	Diatoms	Pichon (1985)

Table 2. Description of all the simulations through their name, the value of the WAIS fwf applied, the use of data assimilation (or not) and the target period (8 or 10 ka).

Name	WAIS fwf (Sv)	Data assimilation	Date of the snapshot
STD 8	50 mSv	No	8 ka
STD 10	50 mSv	No	10 ka
ATM 8	50 mSv	Yes	8 ka
ATM 10	50 mSv	Yes	10 ka
varFWF8	Variable	Yes	8 ka
varFWF10	Variable	Yes	10 ka
FWF 8	120 mSv	No	8 ka
FWF 10	25 mSv	No	10 ka
ATMFWF 8	120 mSv	Yes	8 ka
ATMFWF 10	25 mSv	Yes	10 ka

Table 3. Root mean square error (RMSE) in ˚C of the various simulations (STD, ATM, FWF and ATMFWF) for Antarctic and the oceanic Southern Ocean temperatures. For each region and experiment, the RMSE is computed by the square root of the average of the squares of the deviations between 8 – 10 ka anomalies from reconstructions and model at the same location. Records considered as Antarctic records or Southern Ocean records are described in Tables 1a and b.

Experiments	Antarctica	Southern Ocean
STD	1.01	1.28
ATM	0.45	1.05
FWF	0.74	0.73
ATMFWF	0.38	0.61

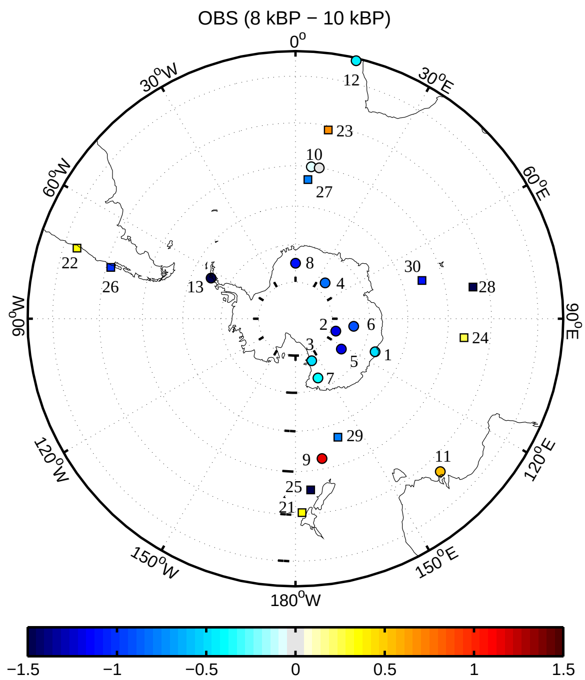

Fig. 1. Available early Holocene temperature data at high southern Latitude. Colors show the temperature differences between 8 and 10 ka. Circles correspond to the proxy data used in the simulations with data assimilation. Squares depict available proxy data that are not used in the simulations with data assimilation, because of either low resolution or not covering the reference or fossil periods (cf. Sect. 2.3 for more explanation). Both types of data are taken into account to validate the simulations. A description of these proxies is show in Tables 1a and b.

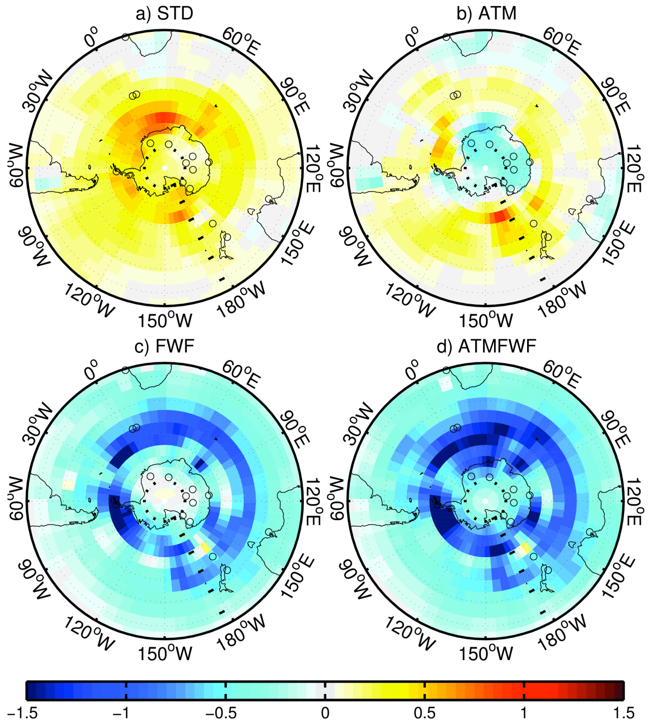

Fig. 2. Difference of the annual mean atmospheric surface temperature between 8 and 10 ka for **(a)** STD, **(b)** ATM, **(c)** FWF, **(d)** ATMFWF.

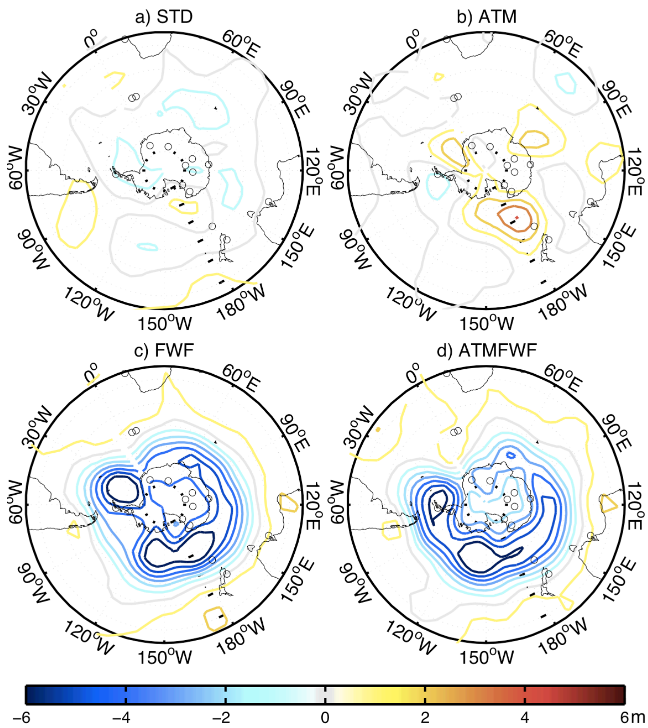

Fig. 3. Difference of annual geopotential heigh at 800 hpa (in m) between 8 and 10 ka. **(a)** STD, **(b)** ATM, **(c)** FWF, **(d)** ATMFWF.

Discussion Paper | Discussion Paper | Discussion Paper | Discussion Paper |

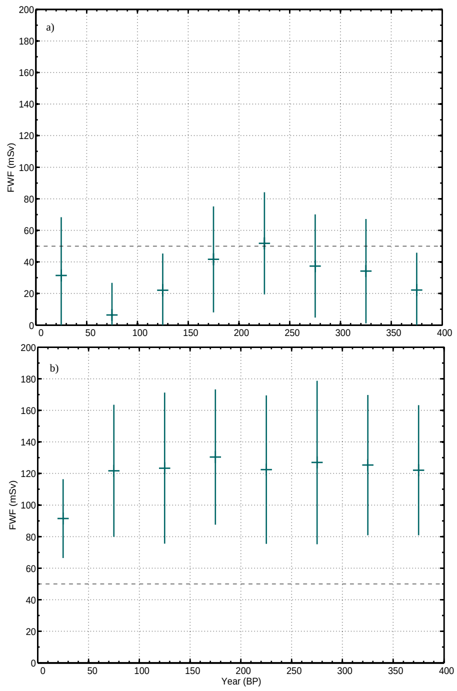

Fig. 4. Reconstruction of fwf based on data assimilation for 10 ka (varFWF10 simulation) **(a)** and 8 ka (varFWF8 simulation) **(b)**. For each time step (50 yr), the green cross is the mean value and green bar is the standard deviation. The x-axis is the time since the beginning of the experiments. The dashed line is the reference value in 8 and 10 ka.

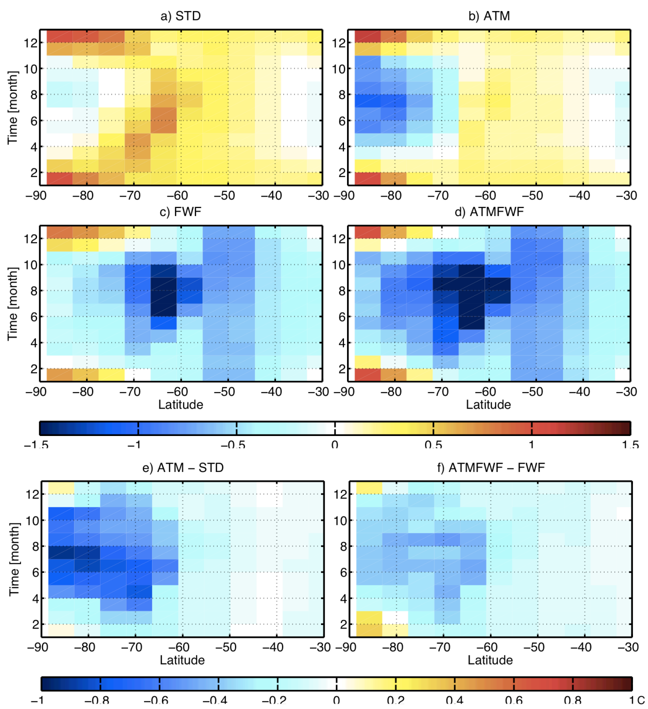

Fig. 5. Zonal mean temperature differences in °C between 8 and 10 ka for STD **(a)**, ATM **(b)**, FWF **(c)**, ATMFWF **(d)**. The difference between the data presented in panels **(b)** and **(a)** (**d** and **c**) is plotted on panel **(e)** (and **f**). Labels on the y-axis correspond to the beginning of the month. Note the different color bar for panels **(a)**–**(d)**.

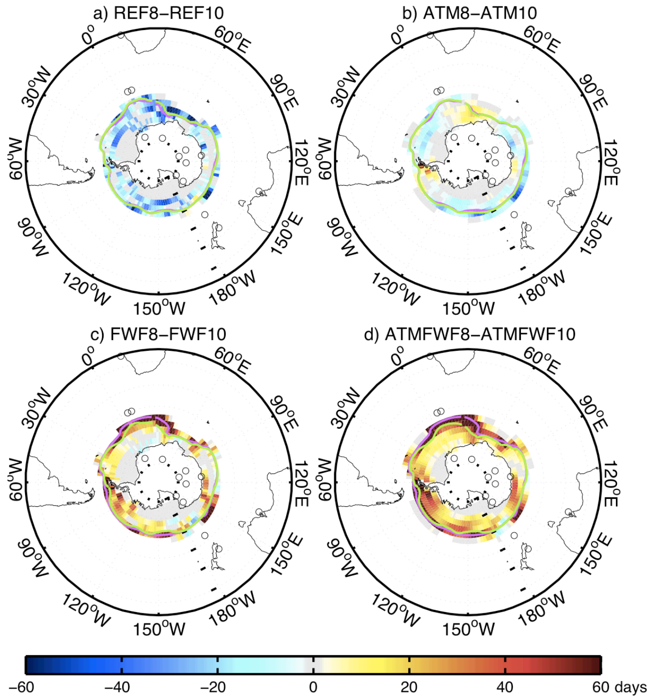

Fig. 6. Difference of sea-ice duration between 8 and 10 ka (expressed in days) in **(a)** STD, **(b)** ATM, **(c)** FWF, **(d)** ATMFWF. Pink (green) lines show the sea-ice extent during September in 8 ka (10 ka). Grey areas along the Antarctica coast show locations where annual sea ice is present in both periods.